



ALMA MATER STUDIORUM  
UNIVERSITÀ DI BOLOGNA

ARCHIVIO ISTITUZIONALE  
DELLA RICERCA

## Alma Mater Studiorum Università di Bologna Archivio istituzionale della ricerca

Constructal design of passive micromixers with multiple obstacles via computational fluid dynamics

This is the final peer-reviewed author's accepted manuscript (postprint) of the following publication:

*Published Version:*

Cunegatto E.H.T., Zinani F.S.F., Biserni C., Rocha L.A.O. (2023). Constructal design of passive micromixers with multiple obstacles via computational fluid dynamics. INTERNATIONAL JOURNAL OF HEAT AND MASS TRANSFER, 215, 1-15 [10.1016/j.ijheatmasstransfer.2023.124519].

*Availability:*

This version is available at: <https://hdl.handle.net/11585/937553> since: 2023-07-31

*Published:*

DOI: <http://doi.org/10.1016/j.ijheatmasstransfer.2023.124519>

*Terms of use:*

Some rights reserved. The terms and conditions for the reuse of this version of the manuscript are specified in the publishing policy. For all terms of use and more information see the publisher's website.

This item was downloaded from IRIS Università di Bologna (<https://cris.unibo.it/>).  
When citing, please refer to the published version.

(Article begins on next page)

# **CONSTRUCTAL DESIGN OF PASSIVE MICROMIXERS WITH MULTIPLE OBSTACLES VIA COMPUTATIONAL FLUID DYNAMICS**

Eduardo Henrique Taube Cunegatto – [eduardohtc@edu.unisinos.br](mailto:eduardohtc@edu.unisinos.br)

Flávia Schwarz Franceschini Zinani – [fzinani@unisinos.br](mailto:fzinani@unisinos.br) (*Corresponding author*)

Mechanical Engineering Graduate Program, Universidade do Vale do Rio dos Sinos (UNISINOS). Av Unisinos 950, 93022-000 São Leopoldo, Brazil.

Cesare Biserni – [cesare.biserni@unibo.it](mailto:cesare.biserni@unibo.it)

Department of Industrial Engineering (DIN), Alma Mater Studiorum, University of Bologna. Viale Risorgimento 2, 40136 Bologna, Italy.

Luiz Alberto Oliveira Rocha – [luizrocha@mecanica.ufrgs.br](mailto:luizrocha@mecanica.ufrgs.br)

Mechanical Engineering Graduate Program, Universidade Federal do Rio Grande do Sul (UFRGS). Rua Sarmiento Leite 425, 90040-001 Porto Alegre, Brazil.

## **Abstract**

Passive micromixers have applications mainly in the chemical, pharmaceutical, and materials industries. Two or more fluids mix while flowing through microchannels in these devices. Due to the small dimensions and low flow rates, the flow is essentially laminar, and mixing takes place mainly by mass diffusion. One way to increase the mixing rate in micromixers is the addition of obstacles that increase the advective effects. This work aimed to introduce high-performance designs of passive micromixers with multiple obstacles. These designs were obtained by combining the Constructal Design method with the Response Surface Optimization method and Computational Fluid Dynamics (CFD). The micromixers were Y-shaped tubes with grooves and circular obstacles in cells that repeated along the device. From the first design inspired by a high-performance design from the literature, the evolutionary design of the system was achieved by increasing the number of obstacles and finding the best configuration for each evolution level (number of obstacles per cell, from three to seven). The effects on mixing percentage, pressure difference, and mixing energy cost (*MEC*) of obstacles' vertical and horizontal distances were investigated with CFD simulations. Increasing the number of obstacles made it possible to increase the mixture percentage of the micromixer. At the same time, the total pressure drop rises faster than the mixing percentage. However, analyzing the pressure locally, it was shown that the lower the

number of obstacles, the greater the local pressure drop, which could cause flow obstructions. The vertical distance of the obstacles had a more significant impact on the mixing than their horizontal distance. Both vertical and horizontal distances had a substantial effect on the pressure drop. As the number of obstacles increased, the effect of the horizontal distance became weaker as its variation was limited. The three-obstacles design presented a *MEC* equal to 2.47 and a mixing percentage equal to 67.12% mixing index. The latest design evolution (i.e., seven obstacles) achieved the best mixing percentage, 70.30%, with *MEC* equal to 2.97. By modifying the degrees of freedom, it was possible to understand and propose a path to the evolutionary design of the system to increase its performance while still using simple designs.

**Keywords:** *Constructal Design; Evolutionary Design; Computational Fluid Dynamics; Microfluidics; Micromixers.*

## 1 INTRODUCTION

Microfluidics is the fluid mechanics field that studies fluids' behavior on small scales, from millimeters to micrometers (Lee and Fu, 2018). Due to the compact size of devices in this field, many application opportunities are emerging, such as pathogen detection in food (Lonchamps et al., 2022), microfluidic sensors (Li et al., 2022), and organ-on-a-chip (Saorin, Caliguri, and Rizzolio, 2022). Thus, microfluidics is a strategic area for engineering, chemistry, computing, and health evolution.

Micromixers are one of the most used devices in microfluidics. Such devices mix two or more liquid substances isolated or coupled on a chip. The range of applications is varied, with examples in the chemical, biological, and medical areas involving diagnosing diseases and producing pharmaceuticals and new materials (Li et al., 2022). Chips coupled with micromixers are used in many applications. One of the most important nowadays is the lab-on-a-chip, a device that conducts laboratory functions on a miniaturized scale. Another example is the organ-on-a-chip, which combines biological and microtechnological aspects to reproduce aspects of human physiology via microchannels that guide and manipulate solutions (Leung et al., 2022).

The devices may employ two distinct mixing mechanisms: active and passive. The first uses external forces, such as electromagnetic fields, sound waves, electric fields, or heat transfer (Li et al., 2022). By using such a methodology, it is possible to achieve high mixing rates and have greater control of the process through the intensity of the applied

flow. However, external devices and energy are required, which can become a hindrance depending on the application.

In passive micromixers, two or more different fluids enter the device through separate inlets and flow through a mixing channel. The fluids are expected to mix by the molecular diffusion mechanism while they flow through the channel. The flow system design may enhance the mixing by adding advection and mixing by disturbing the main flow. For example, curved channels, obstacles, baffles, and indentations are usually employed in different shapes designed to increase mixing in the flow that is fundamentally laminar due to the device's small size. Conversely, as the flow is disturbed to increase mixing, the pressure difference required to maintain the flow rate can greatly increase. Thus, the design of geometries for micromixers seeks to optimize the conflicting objectives of mixing and flow resistance.

Cai et al. (2017) extensively reviewed micromixers, encompassing active and passive devices. In this article, the authors cite numerous papers addressing mixing efficiency as a function of passive micromixer design. The authors highlight the role of 3D printing manufacturing processes, which have boosted the development of microdevices with increasingly complex geometries with more precision, less time, and less cost.

Micromixer performance analysis can be done experimentally and via simulation models. Computational Fluid Dynamics (CFD) has been used to simulate micromixers using distinct numerical methods. Experimental methods can be challenging and limited, considering the difficulty and cost of prototyping and sensing. Using computational simulation methods, for example, CFD, presents virtually no restrictions, allowing a wide variety of cases to be evaluated quickly. However, the results of CFD models must be appropriately validated by comparison with experiments. In the literature are present numerous works with experimental, numerical applications and association of both, enabling the verification and validation of numerical models, such as the studies of Wang et al. (2012), Khaydarov, Borovinskaya and Reschetilowski (2018), and García, Mousaviraad, and Saraji (2022). Santana et al. (2019), using CFD, introduced a new micromixer design (MTB – micromixer with triangular baffles and circular obstructions) aiming the combination of three mass transfer enhancements mechanisms: reduction of molecular diffusion path, split and recombination of streams and vortex generation. This work obtained optimal configurations considering mixtures of vegetable oil/ethanol and water/ethanol, and a wide range of Reynolds numbers, from 0.1 to 100. The objective

functions for optimization were the mixing performance and the pressure drop. This work corroborates the use of obstacles to obtain high-performance micromixers. Antognoli et al. (2021) employed optimized obstacles (pillars) sequences in T-microchannels to improve the mixing of miscible fluids of similar density and viscosity. In further work, Antognoli et al. (2023) performed investigations aiming for more realistic mixing applications, employing fluids with significantly different fluid properties. They studied how fluid velocity and the obstacles configurations affected the formation of horseshoe vortices, which were the main mixing flow structure. They analyzed water-water, and water-ethanol mixtures at Reynolds numbers from 10 to 100, showing efficiency and pressure drop dependence on physical properties. These works give strong motivation for the use of micromixers with obstacles.

Since mixing performance and pressure difference are highly sensitive to the micromixer geometry, advanced optimization methods, coupled with CFD simulation, have been employed to develop new and better micromixer designs. The authors Chen and Lv (2022) presented a brief review of previous works that used different optimization tools for different ideas of micromixer design. In their work, these authors employed Cantor fractal theory in designing obstacles for a passive micromixer, aiming to find the design that would result in the highest mixing rate and lowest pressure difference. Optimization techniques such as Response Surface Analysis (RSA) and a multi-objective genetic algorithm were combined. The results showed that using the genetic algorithm and the Pareto curve analysis effectively obtained optimal designs. Using these techniques, the authors improved the mixing rate by 21% and 14% when operating with Reynolds numbers equal to 1 and 10, respectively. Furthermore, applying fractal theory in micromixer design proved an assertive alternative since high mixing rates and low-pressure differences were obtained. Santana et al. (2022) introduced a method for design, optimization, and prototyping micromixers inspired by plate column trays with high mixing efficiency. The authors used CAD modeling, Design of Experiments (DoE), and CFD to obtain the best designs. The optimal configuration was scaled-up, and a prototype was manufactured by 3D printing and used in the experimental synthesis of (Z)-5-(4-hydroxy benzylidene)thiazolidine-2,4-dione (HBT), obtaining competitive results and showing the practical applicability of the design method by optimization based on CFD. Hasheminejad and Fallahi (2022) investigated using CFD, a flow-mixing methodology that uses vortex-induced vibrations (VIVs) of elastically-suspended cylinders. The authors studied the effects of mixer cross-sectional shapes (circular, square, tilted square,

tilted elliptical, and vertical elliptical), channel blockage ratio, and velocity on mixing performance. The best performances for the stationary vertical elliptical and tilted square cylinders in narrow channels were achieved. At the same time, the VIV-based mixing designs did not lead to appreciable improvements in the mixing performance for those specific geometries. These findings indicate that high-performance micromixers can be designed by obstacle shape optimization.

Adrian Bejan established the Constructal Theory in 1996 (Bejan, 1997). According to this theory, which was further explained and explored by Bejan and Lorente (2008) and many other books and articles, we understand that living systems evolve their configurations to facilitate access to the flows that keep them alive (Bejan and Lorente, 2008). Thus, many engineering works have used a design method for thermal and flow systems called Constructal Design Method (CDM) (Bejan and Zane, 2012, Rocha, Lorente and Bejan, 2018, Borahel et al., 2022, and references therein). This method consists of identifying the flows that keep the system alive, i.e., the purpose of that system. These flows must be facilitated for the system's best performance. Then the degrees of freedom (parameters) and constraints for the metamorphosis of the system are defined, and the effects of the parameters on the system's performance are determined. Thus, it seeks to evolve designs from basic to better performance forms.

The application of CDM in the analysis of passive micromixers is scarce. The work by Cetkin and Miguel (2019) was the most relevant and similar to the ideas developed in the present study. The authors evaluated three passive micromixer designs - branched duct systems, branched ducts with spherical mixing units, and branched ducts with obstacles - regarding higher mixing and lower flow impedance, the latter parameter being a unique perspective in micromixer analysis. Concerning the first design, the authors identified that a longer, larger diameter main channel performs better. The other configurations showed higher mixing rates but higher impedance as well. Although, for a given flow impedance, the first design provides better mixing efficiency. All those designs were developed for volume-constrained systems, corroborating with Constructal Theory principles and thus offering an innovative way to evaluate micromixing devices.

Among the works that motivated this study, we cite that of Ortega-Casanova (2017), who applied the Response Surface Method (RSM) to optimize the geometry of a T-type micromixer with two-bar mixing units. Starting from a reference geometry, the authors determined degrees of freedom, varying geometry parameters via computer simulation until an optimal configuration was obtained. Authors Rahmenezhad and

Mirbozorgi (2019) performed a multiobjective analysis via CFD and RSM on a Y-type grooved micromixer with different obstacle shapes – circular, diamond square, seeking the highest mixing rates and lowest energy costs (pressure difference). They successfully obtained geometries that met the objectives for each obstacle shape. This idea was further improved by Mainochi et al. (2022) using machine learning tools. A neural network algorithm was used to train the data with the evaluated parameters, while a genetic algorithm was used to find the best geometry (high mixing and low pressure). Finally, Nikpour and Mohebi (2022) combined CFD, RSM, and different meta-heuristic algorithms for multi-objective optimization. They obtained satisfactory results in designing passive Y-type micromixers with obstructions, sharing a similar design with the previous works. The authors provided an insightful analysis of different multi-objective optimization algorithms and identified the best one that suited their objectives. They found that diamond-shaped obstacles performed the best in mixing index and pressure difference.

The present work proposes the evolution of micromixers from the designs introduced by Rahmannedzhad and Mirbozorgi (2019) and Mainochi et al. (2022). Thus, the Constructal Design method, coupled with the Response Surface method and CFD, is used as a methodology of an evolutionary design for high-performance passive micromixers. For this, the geometry optimized by Mainochi, et al. (2022) is taken as a reference, and the design evolution, i.e., design change of a flow system with freedom to morph (Bejan, 2016), is proposed.

## **2 METHODOLOGY**

### **2.1 Constructal Design Method**

The Constructal Design Method was used to design micromixers based on the workflow depicted in Figure 1. The method assumes the definition of a finite size system, the identification of the flow is the purpose of the system, i.e., which keeps the system alive, the definition of a performance indicator, the definition of constraints and degrees of freedom, evaluation of configurations, and a method for the identification (optimization) of the best-performing designs. The method was lightly adapted from the workflow presented by Borahel et al. (2022) and Cunegatto, Gotardo, and Zinani (2023).

**It follows the steps detailed below.**

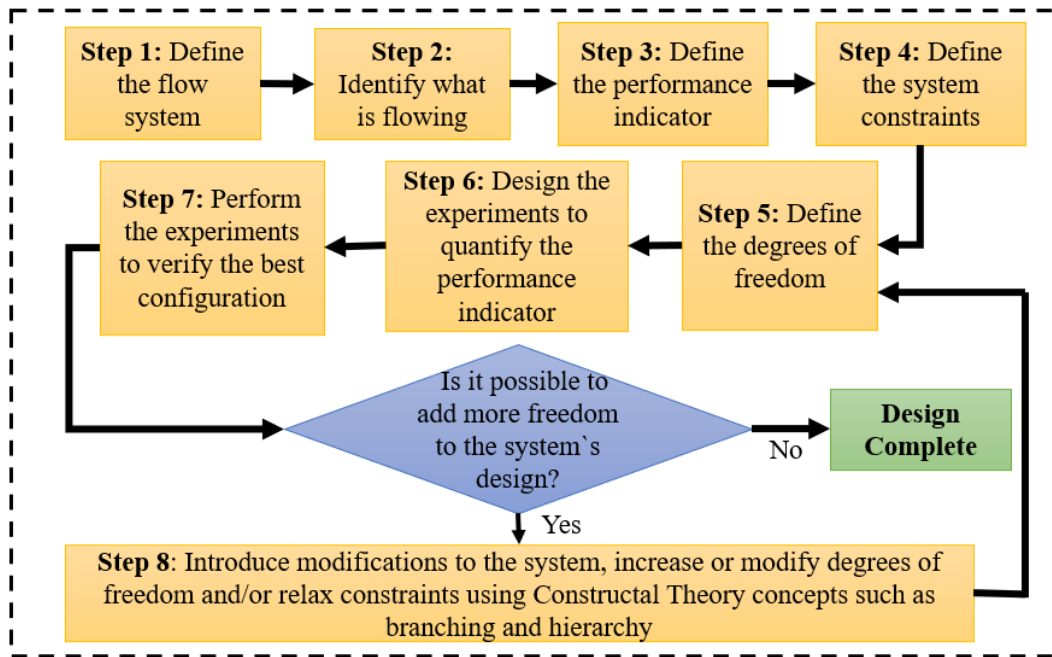


Figure 1 – Constructal Design Method workflow.

### Step 1: Flow system

The system under analysis is a **two-dimensional** micromixer, whose reference design was proposed by Mainochi et al. (2022). Two distinct species enter the device via two separate inlets and mix while they flow in the direction of the outlet, as shown in Figure 2(a). The micromixer is divided into two main sections: the Y-shaped inlets and the channel. A different species enters the device at the same speed at each inlet. The mixing process occurs in the mixing channel, which is 20 mm long and 200  $\mu\text{m}$  wide. The channel comprises semicircular structures – grooves – and circular obstacles responsible for changing the flow path and enhancing mixing. The region between every two following grooves is considered a cell. Grooves are separated by 1000  $\mu\text{m}$ . Figure 2(b) represents the alternative design introduced to improve the reference design. The idea is to keep the area occupied by the obstacles constant (and equal to 0.256  $\text{mm}^2$ ), and to increase the number of obstacles from the initial configuration, in which there is a total of 19. In the reference configuration, the obstacles are off-centered by 20  $\mu\text{m}$ , as this was the best design found by Mainochi et al. (2022). In new configurations, the positions of the obstacles are defined by horizontal and vertical distances among them, denoted by  $H$  and  $V$ , respectively, followed by a number that represents the number of obstacles in each cell at each configuration. The obstacles are placed in staggered configurations, centered by the channel centerline.



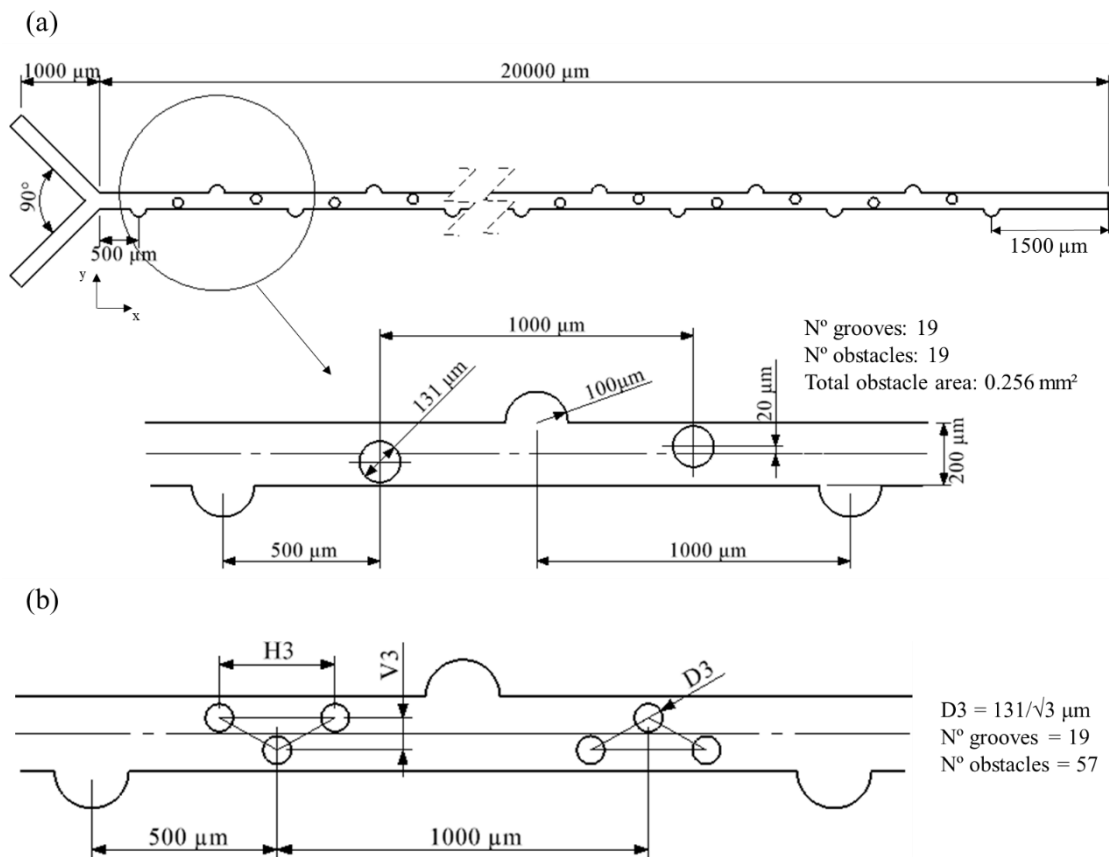


Figure 2 – Schematic drawing of the geometry: (a) General information of the reference geometry; (b) General information of the proposed geometry.

### Step 2: Flow and system's purpose

The system promotes mixing between the two species that flow through the channel. According to Constructal Theory, systems evolve to facilitate the flows that keep them alive. Thus, the flow to be eased is the advective-diffusive flow of mixing species.

### Step 3: Performance indicator

Usually, the parameter used to evaluate the performance of a micromixer is the mixing percentage ( $\phi$ ), which is measured by the concentration profile in a vertical section of the main channel. We use this indicator in the present work. In this case, the position for measurement and evaluation is the outlet boundary of the micromixer. Mathematically, the mixing percentage is expressed by:

$$\varphi = \left(1 - \frac{\sigma}{\sigma_{max}}\right) \cdot 100 [\%_{mix}] \quad (1)$$

where  $\sigma$  represents the standard deviation and the subscript *max* indicates the maximum standard deviation, which is 0.5 for a mixture of two species. The expression used to calculate the standard deviation is:

$$\sigma = \sqrt{\frac{1}{N-1} \sum_{j=1}^N (C_j - \bar{C}_j)^2} \quad (2)$$

where  $N$  is the number of sample points in the vertical section,  $C_j$  is one species concentration in a  $j$  point, and  $\bar{C}_j$  is the average value of the concentration of that species in that section:

$$\bar{C}_j = \frac{\sum_{j=1}^N C_j}{N} \quad (3)$$

However, configurations that improve mixing percentage usually increase the pressure difference ( $\Delta P$ ) along the channel, increasing flow resistance, and possibly impairing the flow. Thus,  $\Delta P$  can also be a performance indicator of ease to flow: the lowest  $\Delta P$ , the easiest the flow. In addition, it is helpful to define an alternative performance indicator. Ortega-Casanova (2017) has introduced the Mixing Energy Cost (*MEC*) design parameter for micromixers. *MEC* is defined as:

$$MEC = \frac{Q_v \Delta P}{\varphi} \left[ \frac{W}{\%_{mix}} \right] \quad (4)$$

where  $Q_v$  represents the flow rate. Reducing the *MEC* is a way to simultaneously improve the mixing rate and pressure difference for a constant flow rate. So, in the present work, we analyze the system's performance regarding  $\varphi$ ,  $\Delta P$ , and *MEC*.

#### **Step 4: Constraints**

The system constraints are the area occupied by the obstacles and the mixer dimensions, as described in Figure 2(a). In addition, we restrict obstacle positions to guarantee that they do not overlap or occupy the spaces under or above the grooves, i.e., they can only occupy the main channel.

#### **Step 5: Degrees of freedom**

We propose to keep the area occupied by obstacles constant and to vary the number of obstacles per cell. For each number of obstacles per cell, the degrees of freedom are the horizontal and vertical distance between two co-linear obstacles. These are denoted by  $H$  and  $V$ , respectively, followed by the number of obstacles in a cell for that specific case. Each configuration, given by a certain number of obstacles per cell, and their distances,  $H$  and  $V$ , is replicated along the mixing channel.

#### **Step 6: Design of experiments (simulations)**

The experiments to evaluate the system's response to parameter changes were done by numerical simulation (CFD). The system response variables were the mixing percentage and pressure difference, while the parameters were the degrees of freedom (horizontal and vertical distances) at each level of system evolution. The Design of Experiments (DOE) was carried out using the Central Composite Design (CCD) method. This method consists of a  $2^k$  factorial model, an axial model, and a central point, where  $k$  represents the number of factors (parameters/degrees of freedom). The distribution of the points of the CCD method allows, with few experiments (simulations), to have a general idea of the behavior of the response variable within the experimental space. Thus, the CCD was used to perform a screening in the search space to find the optimal configuration. Once such a configuration was found, a simulation was performed to assess whether the value predicted by the model was reliable. If the value was outside the curve, a new surface, including the previous optimal point, was generated to evaluate a new optimum. The process was repeated until both predicted and simulated values were agreed. This methodology was applied through the R Statistic programming language via the RStudio programming environment. Table 2 presents the values used in the configuration of the CCD model to create the experimental space for the case of three obstacles per cell.

Table 1- Factor values used in the initial CCD screening space.

| Variable             | Levels    |           |         |            |            |
|----------------------|-----------|-----------|---------|------------|------------|
|                      | Low Axial | Low $2^k$ | Central | High $2^k$ | High Axial |
|                      | Level     | Level     | Level   | Level      | Level      |
| V3 [ $\mu\text{m}$ ] | 50        | 57.32     | 75      | 92.68      | 100        |
| H3 [ $\mu\text{m}$ ] | 200       | 258.58    | 400     | 541.42     | 600        |

The Response Surface Method (RSM) consists of creating a metamodel capable of predicting the behavior of the response variable from the results of experiments performed on specific combinations of parameters. Optimization via RSM is obtaining the optimal configuration through the generated metamodel (Montgomery, 2012). The advantage of RSM is that, in addition to determining a global optimum, it also allows the effects of independent variables and their interactions on the system response to be evaluated, called response surface. The mathematical models commonly employed are second-order regressions, whose solution can be obtained using least squares (Washington, 2011). The quality of the model fit is attested by the parameters *MAE* (mean absolute error), which represents the absolute difference between the results of the experiments and the model, and R-Squared or  $R^2$  (coefficient of determination), which determines how well the model fits the experimental results (El Hami and Pougnet, 2020). It should be noted that the results of the experiments, in the present case, were the results of numerical simulations. The values of  $R^2$  and *MAE* were calculated, respectively, by:

$$R^2 = 1 - \frac{\sum_{i=1}^m (\varphi_{CFD_i} - \varphi_{RSM_i})^2}{\sum_{i=1}^m (\varphi_{CFD_i} - \overline{\varphi_{CFD_i}})^2} \quad (5)$$

$$MAE = \frac{\sum_{i=1}^m |\varphi_{RSM_i} - \varphi_{CFD_i}|}{m} \quad (6)$$

where  $\varphi$  represents the mixing percentage (response variable), and the subscripts RSM and CFD represent the values predicted by the regression model and the simulated values, respectively;  $m$  represents the number of simulated data used to build the model. The bar in the denominator of Equation 5 indicates the mean value of the variable.

### **Step 7: Experiments/simulations**

The mixing percentage and pressure difference for each numerical simulation necessary in the DOE was determined using ANSYS Fluent 2022R2 CFD software based on the Finite Volume Method (Patankar, 1980).

### **Step 8: System's evolution**

Constructal theory predicts that for a system to survive, it must facilitate flows, over time, in a way that improves its goal. In this case, the design of a micromixer must change so that its objective, to mix substances, is improved. Based on this principle, we proposed to modify the geometry of Figure 2(b) by increasing the number of obstacles per cell. Therefore, as the number of obstacles per cell increased, their diameter should also change so that the restrictions concerning the finite size of the device and the constant area occupied by the obstacles were satisfied. Therefore, the proposed evolution path is illustrated in Figure 3.

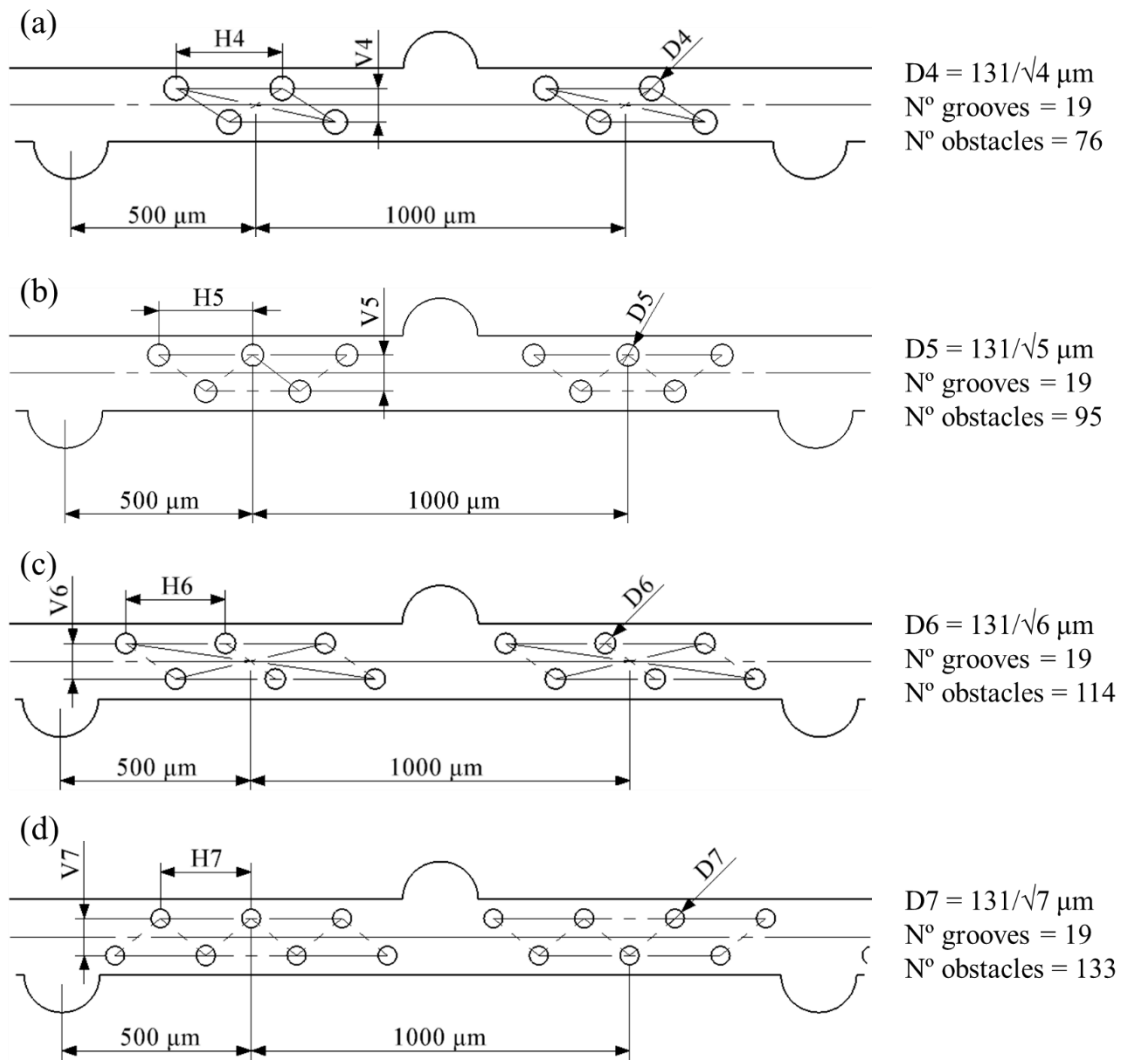


Figure 3 – Schematic drawings of the proposed micromixer system evolution: (a) 4 obstacles; (b) 5 obstacles; (c) 6 obstacles; (d) 7 obstacles.

According to the workflow in Figure 1, the process was repeated according to the steps described above, adjusted to each evolution level. For the proposed evolutions, the adjustments were the new degrees of freedom and the determination of the search space for the new designs; the other steps followed the same procedure. Following the methodology and nomenclature employed in the previous steps, Table 2 presents the search space for the geometries at each degree of evolution, i.e., with each number of obstacles per cell.

Table 2 - Factor values used in the initial CCD screening space for the new geometries.

| Variable | Levels |
|----------|--------|
|----------|--------|

|         | Low Axial<br>Level | Low 2 <sup>k</sup><br>Level | Central<br>Level | High 2 <sup>k</sup><br>Level | High Axial<br>Level |
|---------|--------------------|-----------------------------|------------------|------------------------------|---------------------|
| V4 [μm] | 70                 | 77.32                       | 95               | 112.68                       | 120                 |
| H4 [μm] | 150                | 193.93                      | 300              | 406.06                       | 450                 |
| V5 [μm] | 80                 | 85.86                       | 100              | 114.14                       | 120                 |
| H5 [μm] | 170                | 196.36                      | 260              | 323.64                       | 350                 |
| V6 [μm] | 70                 | 77.32                       | 95               | 112.68                       | 120                 |
| H6 [μm] | 140                | 160.50                      | 210              | 259.50                       | 280                 |
| V7 [μm] | 70                 | 77.32                       | 95               | 112.68                       | 120                 |
| H7 [μm] | 160                | 171.72                      | 200              | 228.28                       | 240                 |

## 2.2 Mathematical modeling

The flow inside the micromixers was modeled via a mixture model. The following equations model the momentum and the mass transfer for the two-dimensional problem domain depicted in Figure 4. These are the mixture mass balance equation, mixture momentum balance equations, and species  $I$  mass fraction equation, given by:

$$\frac{\partial u}{\partial x} + \frac{\partial v}{\partial y} = 0 \quad (7)$$

$$\rho \left( u \frac{\partial u}{\partial x} + v \frac{\partial u}{\partial y} \right) = -\frac{\partial P}{\partial x} + \mu \nabla^2 u \quad (8)$$

$$\rho \left( u \frac{\partial v}{\partial x} + v \frac{\partial v}{\partial y} \right) = -\frac{\partial P}{\partial y} + \mu \nabla^2 v \quad (9)$$

$$\left( u \frac{\partial C_1}{\partial x} + v \frac{\partial C_1}{\partial y} \right) = D_{12} \nabla^2 C_1 \quad (10)$$

where  $u$  and  $v$  are the velocity vector components in directions  $x$  and  $y$ , respectively,  $P$  is the pressure,  $\rho$  is the mixture mass density (998 kg/m<sup>3</sup>),  $\mu$  is the mixture viscosity (8.9.10<sup>-4</sup> Pa.s),  $C_1$  represents the molar concentration of species  $I$ . The concentration of species 2 may be calculated as the molar concentration of all species at a particular place must sum one.  $D_{12}$  is the mass diffusion coefficient (1.10<sup>-9</sup> m<sup>2</sup>/s) and  $\nabla^2$  represents the tensorial relation:

$$\nabla^2 = \frac{\partial^2}{\partial x^2} + \frac{\partial^2}{\partial y^2} \quad (11)$$

As depicted in Figure 4, the boundary conditions associated are the following. Two distinct fluids, 1 and 2, enter the domain via inlets 1 and 2, with uniform velocity and concentration profiles. The velocity at both inlets is  $V_{in}$  and the concentrations are  $C_1$  equal 100% and 0% at inlets 1 and 2, respectively. The microchannel walls and the surface of the obstacles are assumed to be no slip and impermeable. A manometric pressure equal to 0 Pa is prescribed in the outlet section.

The Reynolds and mass Peclet numbers for this problem are given by:

$$Re_W = \frac{\rho W V_{in}}{\mu} \quad (12)$$

$$Pe_W = \frac{W V_{in}}{D_{12}} \quad (13)$$

where  $W$  is the main channel width, 200  $\mu\text{m}$ . The velocity  $V_{in}$  was chosen so that  $Re_W = 1$  and  $Pe_W = 891.8$ , typical ranges found in the literature (Wang *et al.*, 2012; Rahmannedhad and Mirbozorgi, 2019; Chen *et al.*, 2020; Mainochi *et al.*, 2022).

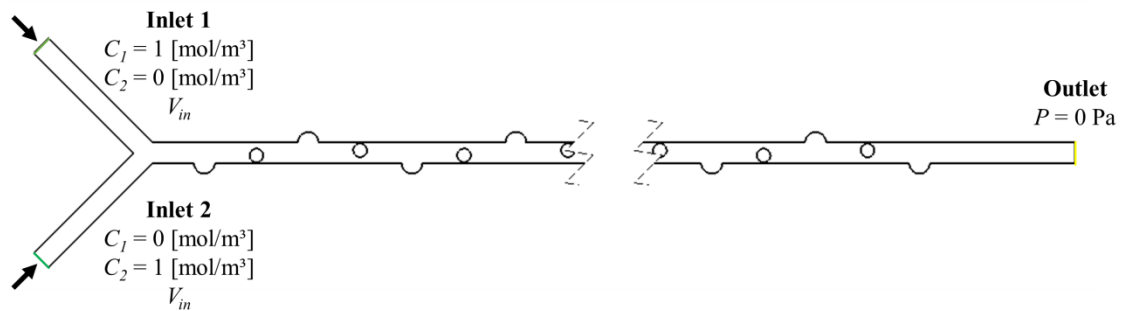


Figure 4 – Scheme for the problem domain and boundary conditions.

### 2.3 Regression models

The regression models used are exploratory and predictive and have been employed in previous works (e.g., Cunegatto, Gotardo, and Zinani, 2023). All the geometries idealized in this work present two independent variables ( $H$  and  $V$ ) for one



dependent variable ( $\varphi$  or  $\Delta P$ ). In this case, a second-order polynomial model was applied, with an interaction term included:

$$\varphi = \beta_0 + \beta_1 H3 + \beta_2 V3 + \beta_3 H3V3 + \beta_4 H3^2 + \beta_5 V3^2 \quad (14)$$

$$DP = \beta_0 + \beta_1 H3 + \beta_2 V3 + \beta_3 H3V3 + \beta_4 H3^2 + \beta_5 V3^2 \quad (15)$$

where  $\beta$  represents the regression coefficients, determined using the least squares method (Washington, 2011).

## 2.4 Numerical method

The mathematical model was solved using the software ANSYS Fluent 2022 R2, using the scheme COUPLED for pressure-velocity coupling, interpolation equations of types PRESTO (Pressure Staggering Option) for pressure, QUICK (Quadratic Upstream Interpolation for Convective Kinematics) for momentum; Third Order MUSCL (Monotonic Upstream-centered Scheme for Conservation Laws) for species concentration. The convergence criteria were  $10^{-6}$  for mass,  $10^{-8}$  for momentum and  $10^{-7}$  for species concentration.

The choice of these models was based on the results of the works of Ortega-Casanova (2017) and Kouadri et al. (2021), which showed higher fidelity using these configurations when compared to experimental data.

### 2.4.1 Computational mesh

The construction of the numerical mesh was based on a standard element size for the main channel. In addition, a prism (inflation) structure was applied around the obstacles to organize the mesh better and capture the flow around these structures. The value adopted for the element size is based on the value employed in the works of Rahmamezhad and Mirbozorgi (2019) and Mainochi et al. (2022), which use Batchelor's Scale methodology as criteria. As per the application of this methodology, the estimated element size value for the works in question is at most  $6 \mu\text{m}$ .

Therefore, for fitting the parameters of the cited studies, the present work used the value of  $5.2 \mu\text{m}$  as a reference for the determination of the mesh element size and, from this value, applied the GCI methodology (CELIK et al., 2008) for evaluation of subsequent refinements. As reported by Ortega-Casanova (2017) and Rahmamezhad and

Mirbozorgi (2019), the mesh significantly influences this type of application, and coarser configurations tend to underestimate the mixture value, justifying the application of the GCI test. The values of the test are presented in Table 3.

Table 3 – Mesh Parameters and Grid Convergence Index (*GCI*) test results.

| <b>GCI - 3-cylinder arrangement – Central point configuration</b> |                    |  |   |                                       |                                   |                                    |
|---|--------------------|--|---|---------------------------------------|-----------------------------------|------------------------------------|
| <b>Mesh</b>   | <b>N° elements</b> | <b>Element size<br/>[<math>\mu\text{m}</math>]</b> | <b><math>\varphi</math><br/>[%<sub>mix</sub>]</b> | <b><math>\Delta P</math><br/>[Pa]</b> | <b><math>GCI_{\varphi}</math></b> | <b><math>GCI_{\Delta P}</math></b> |
| 1 (Fine)  | 479406             | 3.078  | 66.895  | 165.347                               | 2.216% <sub>12</sub>              | 0.464% <sub>12</sub>               |
| 2 (Int.)  | 293022             | 4.000  | 67.998  | 165.035                               |                                   |                                    |
| 3 (Coarse)  | 177530             | 5.200  | 70.179  | 164.554                               | 4.208% <sub>23</sub>              | 0.701% <sub>23</sub>               |

The GCI test was performed on the mixing percentage ( $\varphi$ ) results in the outlet section and the pressure difference ( $\Delta P$ ) between the inlets and the outlet of the micromixer. It can be seen that  $\Delta P$  is little affected by mesh refinements since the maximum value found in the test ( $GCI_{\Delta P}$ ) was 0.701%, indicating that the influence of mesh on this variable is low. Inversely, the effect of mesh on  $\varphi$  is much more significant, reaching 4.216%. This effect has been observed in other works in the literature (Ortega-Casanova, 2017; Kouadri *et al.*, 2021) and is related to the methods to calculate pressure drop and mixing percentage. The area average of a primal variable - the pressure - calculates the pressure drop. The meshes may be considered converged for this variable because they are very fine. However, considering that the data set's mean and standard deviation are used to calculate the mixing percentage, a larger number of points tends to produce more scattered results. Because of this, a more refined mesh has more elements, and similarly, the solution is more distributed, which influences the calculation of the mixing percentage. Thus, we used the most refined mesh (1) depicted in Figure 5.

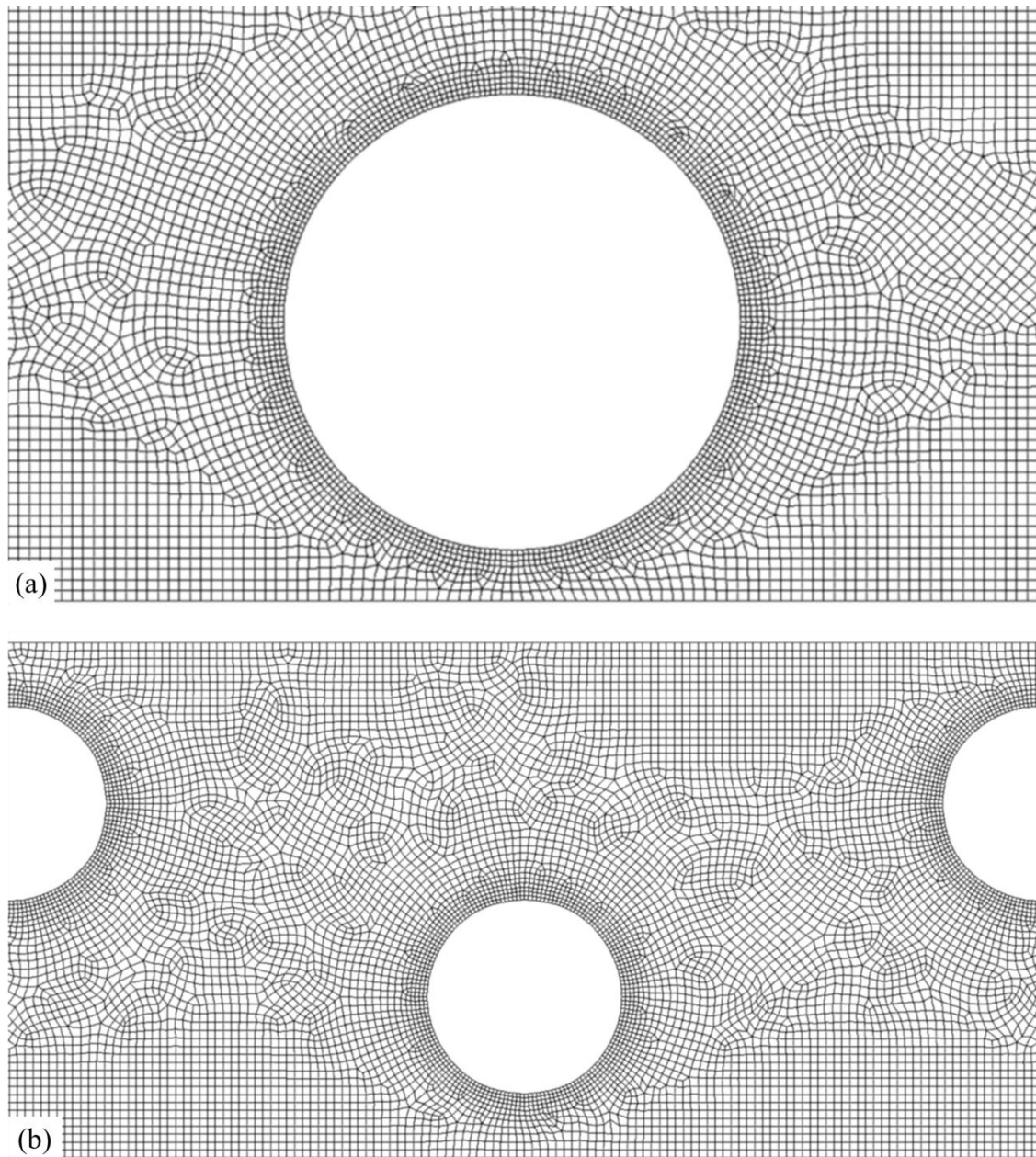


Figure 5 – Computational mesh: (a) Mesh around the obstacle; (b) Mesh between the obstacles.

#### 2.4.2 Model validation

The mathematical and numerical model validation was performed by comparison with the experimental results of Wang et al. (2012), considering the "Design 3" of that work, which is similar to the design in Figure 2 of the present work. The comparison of our numerical results with theirs is exposed in Figure 6. In the graph, the concentration profiles of one species at a specific position in the mixing channel (16 mm from the inlet of the main channel) are confronted. As described in the methodology of Wang et al. (2012), the experimental data were obtained through image analysis of the mixture. By

color difference, it was possible to determine the concentration at each point of the channel cross-section. These results are for Reynolds number equal to one.

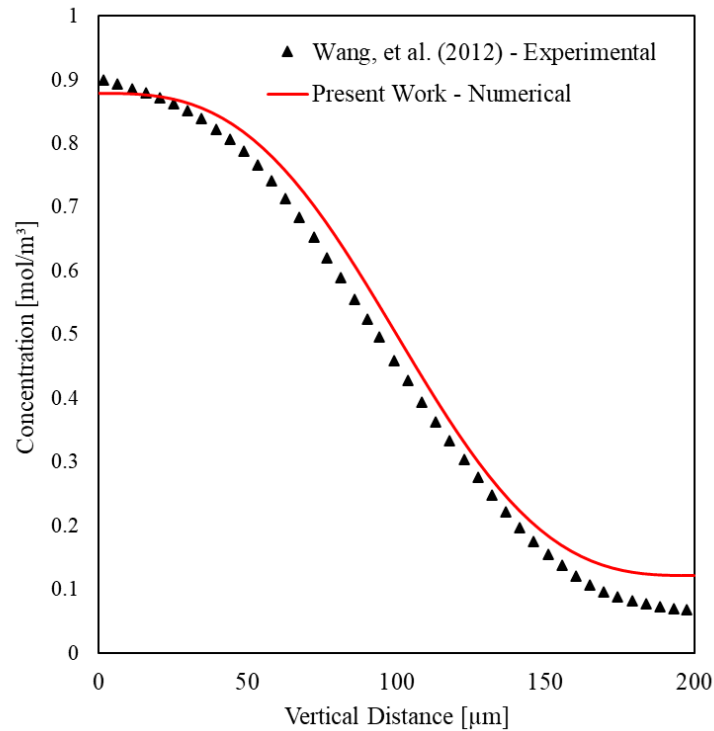


Figure 6 – Validation of the mathematical model comparing the concentration profile of experimental and numerical results.

Figure 6 allows us to observe the agreement between the results. In the low-concentration region, the difference is more pronounced. The numerical simulation predicted a value close to 0.2, while the experiment predicted around 0.1. This difference can be related to numerous factors, such as the numerical mesh, discretization models, or experimental methodology. This difference was also presented in the works of Rahmannedhad and Mirbozorgi (2019) and Mainochi et al. (2022). It is important to note that a flatter profile, i.e., with a smaller concentration difference (lower standard deviation), indicates more mixing. The global numerical result is in good agreement with the experiments. The experimental result for mixing percentage was 39.1% for Wang et al. (2012) and 41.7% for the present work.

We also compared our results with the numerical results of Rahmannedhad and Mirbozorgi (2019), named Ref.1, and Mainochi et al. (2021), named Ref.2, as identified in Table 4. The variables used as a comparison were the pressure difference ( $\Delta P$ ) and mixing percentage ( $\varphi$ ) as a function of obstacle diameter ( $OD$ ) and offset ( $OF$ ), which are the variables studied by the authors. Regarding the former work, four different cases (including the optimized geometry) were compared, while in the latter, only the optimal

configuration was compared. In Table 4, the subscript ref represents the reference result, while CFD represents the result obtained in the present work.

Table 4 – Numerical verification of the results for basic designs.

| Geometric Parameters      |                           | Variable                 |                          |                           |                           | Difference       |                 | Reference     |
|---------------------------|---------------------------|--------------------------|--------------------------|---------------------------|---------------------------|------------------|-----------------|---------------|
| $OD$<br>[ $\mu\text{m}$ ] | $OF$<br>[ $\mu\text{m}$ ] | $\Delta P_{ref}$<br>[Pa] | $\Delta P_{CFD}$<br>[Pa] | $\varphi_{ref}$<br>[%mix] | $\varphi_{CFD}$<br>[%mix] | $\Delta P_{dif}$ | $\varphi_{dif}$ |               |
| <b>110.75</b>             | <b>30</b>                 | <b>143.24</b>            | <b>144.31</b>            | <b>64.00</b>              | <b>62.06</b>              | <b>0.75%</b>     | <b>3.03%</b>    | <b>Ref.1</b>  |
| <b>131</b>                | <b>20</b>                 | <b>227.67</b>            | <b>226.22</b>            | <b>57.98</b>              | <b>58.20</b>              | <b>0.64%</b>     | <b>0.38%</b>    | <b>Ref.2*</b> |
| 90                        | 0                         | 141.27                   | 142.47                   | 54.81                     | 53.66                     | 0.85%            | 2.10%           | Ref.1         |
| 105                       | 22.5                      | 151.14                   | 152.96                   | 62.92                     | 61.00                     | 1.20%            | 3.05%           | Ref.1         |
| 90                        | 30                        | 108.69                   | 109.09                   | 60.14                     | 58.87                     | 0.37%            | 2.11%           | Ref.1         |

Ref.1: Rahmannedhad e Mirbozorgi (2019)  
Ref.2: Mainochi, *et al.* (2022)

\*The results extracted from this reference were obtained at 16 mm from the main channel inlet. The other results were taken at the outlet section of the channel.

The values in bold are for optimized configurations. It can be seen that the most significant differences are in the percentage of mixing, especially about Ref.1. This difference was already expected, mainly because of the numerical mesh, which, as demonstrated by the same authors, has influence depending on the element size (refining), mainly because of the calculation of the standard deviation, necessary to determine the percentage of mixing. **Conversely**,  $\Delta P$  does not present significant differences. About Ref.2, the results are closer, as the mesh and methods employed were more similar. **So, the results exposed here meet the project's scope.**

### 3 RESULTS

#### 3.1 Performance indicators: mixing percentage and pressure difference

The cases studied here represent geometries with two degrees of freedom: vertical distance between obstacles ( $V$ ) and horizontal distance between obstacles ( $H$ ). The response variables used to evaluate the geometries are the mixing percentage ( $\varphi$ ) and the pressure difference ( $\Delta P$ ), assessed at the outlet section of the micromixers. The response surfaces were generated using the second-order model (Equation 11). Figure 7 presents the projections of the response surfaces for  $\varphi$  (left) and  $\Delta P$  (right) for all levels of system evolution, i.e., from 3 to 7 obstacles.

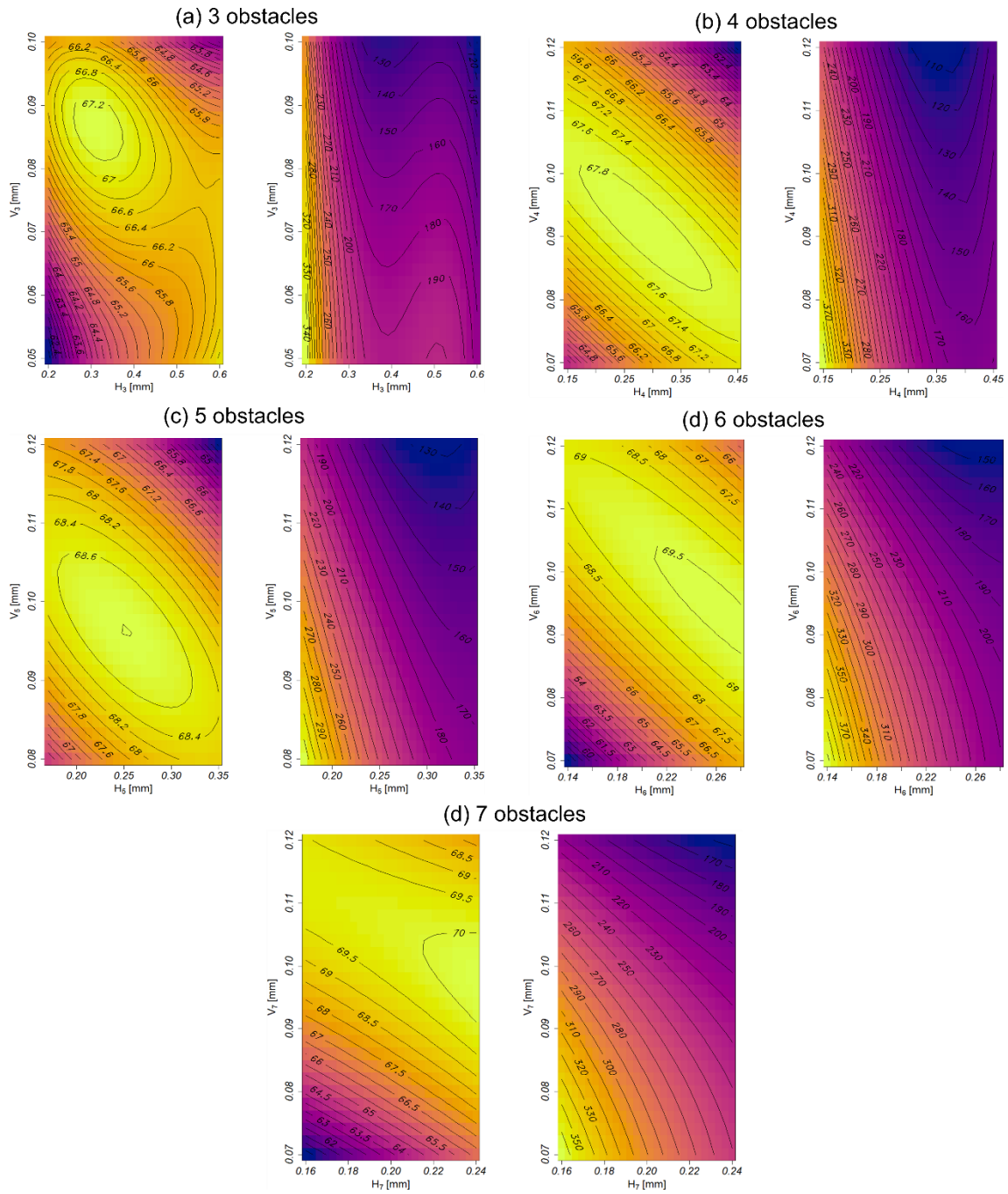


Figure 7 – Response surfaces for the proposed designs regarding mixture percentage (left) and pressure difference (right): (a) 3 obstacles, (b) 4 obstacles, (c) 5 obstacles, (d) 6 obstacles, (e) 7 obstacles.

Regarding the surfaces of the mixing percentage (left), it can be noted that for cases (a), (b), and (c), it was possible to determine an optimal region at the intermediate limits of the experimental field. In contrast, cases (d) and (e) are closer to the maximum  $H$  limit. These results indicate that, in the latter cases, the obstacles should be more horizontally separated to ensure good mixing. Conversely, the modeling of  $\phi$  for the cluster of three obstacles was more complex. Therefore, a third-order model, a simplified

version of the model proposed by Cunegatto, Gotardo, and Zinani (2023), was used to ensure more accurate metrics.

The vertical distance  $V$  has a more significant effect on the results for  $\varphi$  than the horizontal distance  $H$ , and this effect is more important as the number of obstacles increases. In case (e), the effect of  $H$  is minimal since  $\varphi$  varies only with respect to  $V$ .

Regarding  $\Delta P$ , the trend reverses for cases (a) and (b) so that  $H$  has a significant effect, especially at the lower bounds. As  $H$  increases from the region of optimal  $\varphi$ , the effect of  $V$  becomes more important since, from this point on, the obstacles become more separated for larger  $V$  and  $H$ , reducing  $\Delta P$  considerably. The effects of  $H$  and  $V$  are practically equivalent to the other cases. It is important to note that the optimal configuration of mixing percentage is in intermediate regions of the maximum and minimum limits of  $\Delta P$ . The evaluation of the metrics of the models used in generating the response surfaces is presented in the fit plots in Figure 8.

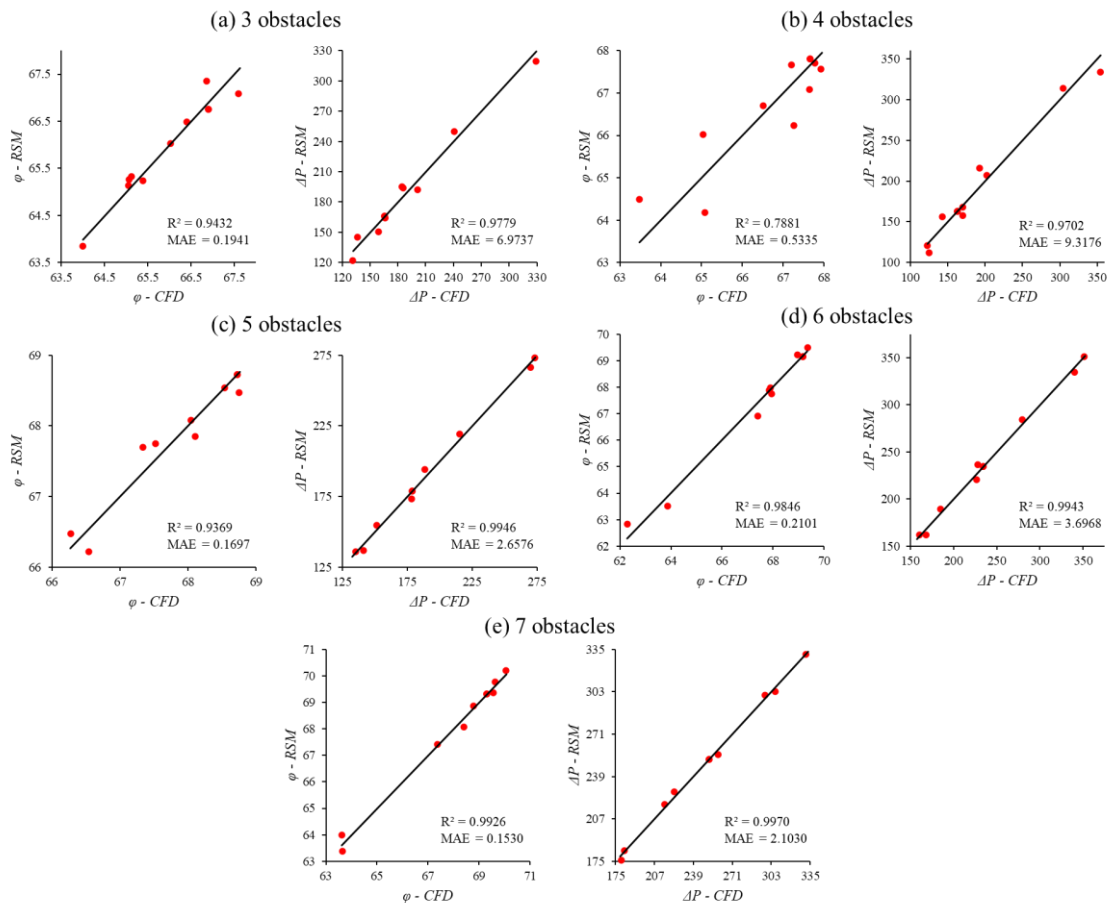


Figure 8 – Fit plots for mixture percentage (left) and pressure difference (right): (a) 3 obstacles; (b) 4 obstacles; (c) 5 obstacles; (d) 6 obstacles; (e) 7 obstacles

The graphs in Figure 8 show that obtaining models with high fit and accuracy was possible. Case (b), referring to the mixing percentage, is the one that presented the worst metrics. It can be observed that the red points tend to be farther from the straight line in the range of values below the maximum, contributing to a lower fit and higher *MAE*. However, points near the region of interest, the maximum, are very close to the line, which is satisfactory.

In case (a), the points are further away from the straight line in the region of maximum, but this difference is slight since the *MAE* is low. The *MAE* values of the graphs of  $\Delta P$  have larger values than those of  $\varphi$  because of the difference in scale. It is important to note that the mathematical models of  $\varphi$  and  $\Delta P$  are of the same order (order three for three obstacles and two for the other cases).

Overall, the models fitted  $\Delta P$  better than  $\varphi$ , indicating that the mixing percentage is more sensitive to the model. Finally, the models obtained sufficient metrics to provide the **work's scope**. The optimal values of  $\varphi$  are shown in Table 5, with their respective  $\Delta P$ .

Table 5 – Table of maximum e optimal values.

| <b>N°<br/>obs.</b> | <b><math>V_{n,opt}</math><br/>[<math>\mu\text{m}</math>]</b> | <b><math>H_{n,opt}</math><br/>[<math>\mu\text{m}</math>]</b> | <b><math>\varphi_{max,CFD}</math><br/>[%<sub>mix</sub>]</b> | <b><math>\Delta P_{CFD}</math><br/>[Pa]</b> | <b><math>\varphi_{max,RSM}</math><br/>[%<sub>mix</sub>]</b> | <b><math>\Delta P_{RSM}</math><br/>[Pa]</b> | <b><math>\varphi</math><br/>diff.</b> | <b><math>\Delta P</math><br/>diff.</b> |
|--------------------|--|--|---|---|---|---|---------------------------------------|--|
| 3                  | 86.8   | 311.6  | 67.12   | 165.48                                      | 67.35   | 162.98                                      | 0.34%                                 | 1.51%                                  |
| 4                  | 91.6   | 287.1  | 67.93   | 174.01                                      | 67.88   | 177.73                                      | 0.07%                                 | 2.14%                                  |
| 5                  | 96.5   | 251.0  | 68.90   | 191.01                                      | 68.80   | 192.14                                      | 0.15%                                 | 0.59%                                  |
| 6                  | 93.9   | 262.6  | 69.55   | 195.82                                      | 69.60   | 197.26                                      | 0.07%                                 | 0.74%                                  |
| 7                  | 98.2   | 240.0  | 70.30   | 208.49                                      | 70.26   | 211.60                                      | 0.06%                                 | 1.49%                                  |

The relative difference between the  $\varphi$  and  $\Delta P$  obtained at the optimal points from the response surfaces by simulation is low, especially for  $\varphi$ . **Conversely**,  $\Delta P$  shows more significant differences, even with more precise metrics, as seen in Figure 8, but still satisfactory.

Regarding the optimal geometric configurations, there is a tendency for vertical spacing to increase and horizontal spacing to decrease as the number of obstacles grows. The *H* spacing decreases because of more obstacles, which limits its range of variation. It is important to note that because of the constant area constraint, the diameter of the obstacles decreases as the number of obstacles increases. Regarding the increase in *V*, this can also be associated with the system's head loss since, as seen in the  $\Delta P$  surfaces, its influence is more significant, especially for a larger number of obstacles. With this, the geometry had to evolve so the flow had room for mixing. Finally, it is noted that  $\varphi$  also



increases as the number of obstacles grows, in the same way as  $\Delta P$ . Figure 9 illustrates the concentration contours in the optimal configurations for each design.

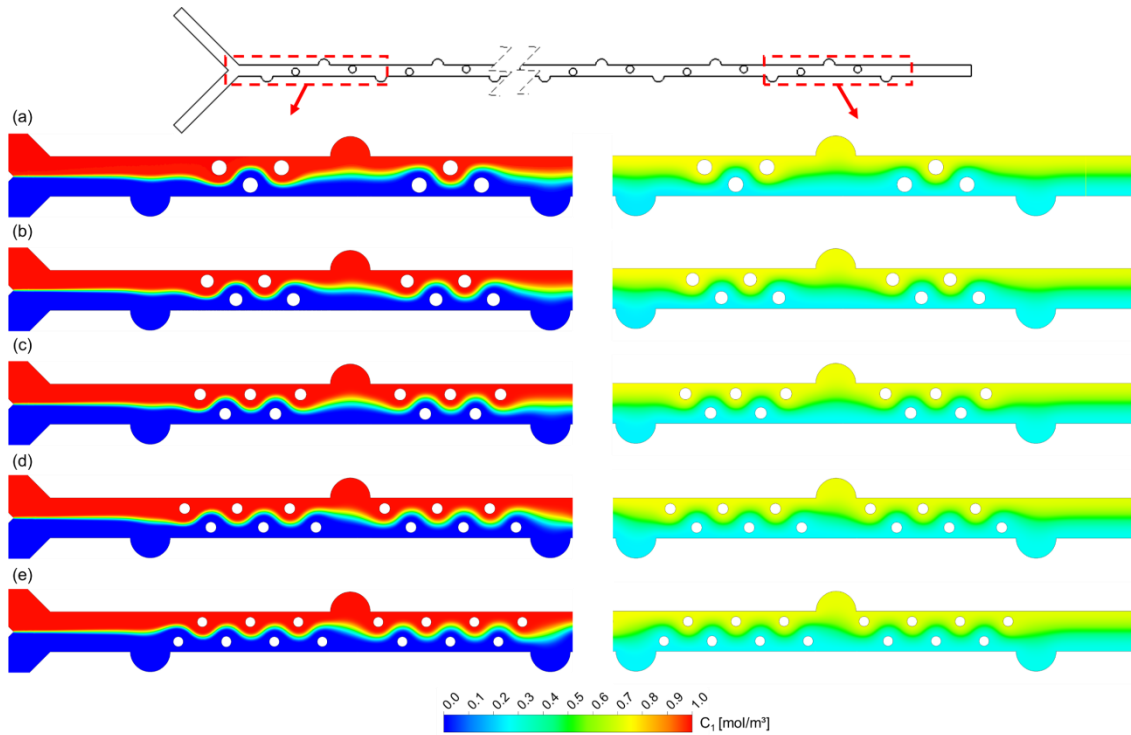


Figure 9 – Concentration contours for each design evolution level at the optimal configuration: (a) 3 obstacles; (b) 4 obstacles; (c) 5 obstacles; (d) 6 obstacles; (e) 7 obstacles.

The concentration contours in the inlet region of the micromixer (left) show that the mixing layer between the two fluids is thin near the channel inlet. As it reaches the first groove, a slight disturbance in the flow occurs, which causes an increase in its thickness. This process intensifies as the mixture enters the "mixing unit" (arrangement of obstacles), which causes more significant disturbances in the flow. Upon reaching the second groove, the concentration layer is thicker than in the first groove, showing the effect of the obstacles on species mixing.

In the outlet section, one notices that the central axis interface is green, indicating 100% mixing. Also, compared to the initial region, there are no longer regions of pure species (red or dark blue) but a mixture gradient along the channel cross-section.

The presence of more obstacles causes more disturbances to the flow, which improves the mixing rate by adding advective effects to an extremely slow flow. However, comparing cases (a) and (e), the difference in concentration is almost imperceptible, so the best design can be indicated only via a percentage of mixing

analysis. In the evolution from (a) to (e),  $\varphi$  increases from 67.4% to 70.3% at the outlet of the micromixer.

### 3.2 Performance indicator: Mixing Energy Cost

The Mixing Energy Cost (*MEC*, Equation (4)) can be used to evaluate the performance of systems after analysis using  $\varphi$  and  $\Delta P$  as response variables. Table 5 was built to evaluate the *MEC* of the best configurations obtained using the RSM, emphasizing the importance of having a high mixing percentage and keeping a low-pressure drop. The first two lines in Table 6 show the optimum results presented by Rahmannedhad and Mirbozorgi (2019) (Ref.1) and Mainochi et al. (2021) (Ref.2). The following lines present the optimal results for  $\varphi$  obtained in the present work.

Table 6 – Mixing Energy Cost comparison of some of the best designs in this work.

| Design               | $\varphi$ [% <sub>mix</sub> ] | $\Delta P$ [Pa] | <i>MEC</i><br>[Pa/% <sub>mix</sub> ] | <i>MEC</i> Diff<br>[%] |
|----------------------|-------------------------------|-----------------|--------------------------------------|------------------------|
| Ref.1 <sub>opt</sub> | 62.06                         | 144.31          | 2.33                                 | -                      |
| Ref.2 <sub>opt</sub> | 58.20                         | 226.22          | 3.87                                 | -                      |
| 3 obstacles          | 67.12                         | 165.48          | 2.47                                 | 6.01%                  |
| 4 obstacles          | 67.93                         | 174.01          | 2.56                                 | 3.65%                  |
| 5 obstacles          | 68.90                         | 191.01          | 2.77                                 | 8.20%                  |
| 6 obstacles          | 69.55                         | 195.82          | 2.81                                 | 1.44%                  |
| 7 obstacles          | 70.30                         | 208.49          | 2.97                                 | 5.69%                  |

Ref.1: Rahmannedhad e Mirbozorgi (2019)

Ref.2: Mainochi, *et al.* (2022)

Table 6 shows that the *MEC* of Ref.1 was below the *MEC* obtained for the optimal configurations in the present work. However, the *MEC* of the optimal design in Ref.2 was above the values in the current work. The range of values obtained in this work is competitive. With the case of 3 obstacles, it was possible to increase, relative to Ref.1, the mixture by 8%, against a 6% increase in the *MEC*, which is a positive indication. The design with four obstacles showed a rise of 9.46% for the mixture and 9.87% for the *MEC*, which already became undesirable. In the cases of 3 and 7 obstacles, there is a 4.74% increase in  $\varphi$ , against 20.24% in *MEC*, showing that the first design (3 obstacles), in terms of *MEC*, is the most efficient. Furthermore, considering the case of Ref.2, whose result was obtained at a distance of 16 mm from the junction point, the design with three obstacles obtained a mixing percentage of 57.10%, with  $\Delta P$  of 136.14 Pa in the same region, a reduction of 39.82%.

The last column of the table shows the difference between the MEC of the corresponding design versus the previous one. For example, the transition between 5 and 6 obstacles showed a difference of only 1.44%, while the most significant difference is between the 4 and 5 obstacle design. Such metrics indicate that one has dramatically increased the overall pressure difference for little mixing percentage, which does not compensate for the use of this design.

The pressure difference analysis in micromixers can be easily performed using CFD since this practice at the experimental level has yet to be verified. Even if the microscale pressure is relatively low, the MEC becomes an important parameter for evaluating micromixer designs.

Some micromixers are employed as reactors to produce micro or nanoparticles. These particulates can accumulate in slow-flow locations, making it increasingly difficult for fluid to pass through, requiring more energy. With that in mind, designs that offer lower resistance to flow ( $\Delta P$ ) can mitigate this effect. This principle is associated with the Constructional Theory perspectives of facilitating the flow and ensuring system survival. Figure 10 depicts the pressure fields for the optimal cases of 3 and 7 obstacles.

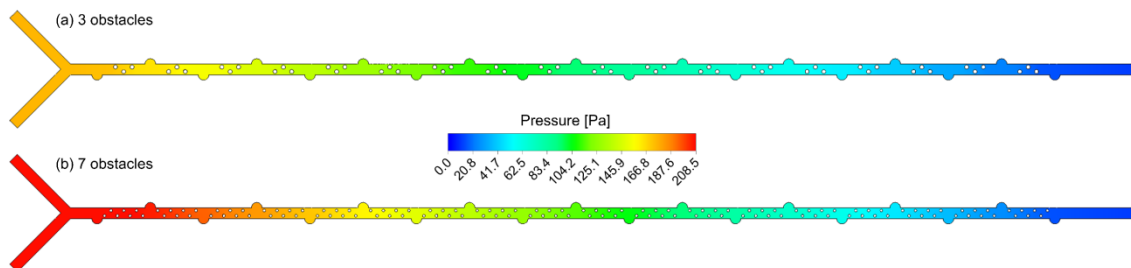


Figure 10 – Pressure contours for the optimal geometries: (a) 3 obstacles; (b) 7 obstacles.

The pressure, in both cases, does not present any specific region of high gradient, presenting a practically uniform distribution along the flow direction. This behavior is beneficial for both designs since, from the images, it is not possible to detect any region of risk for obstructions. The behavior of the pressure difference is presented graphically in Figure 11.

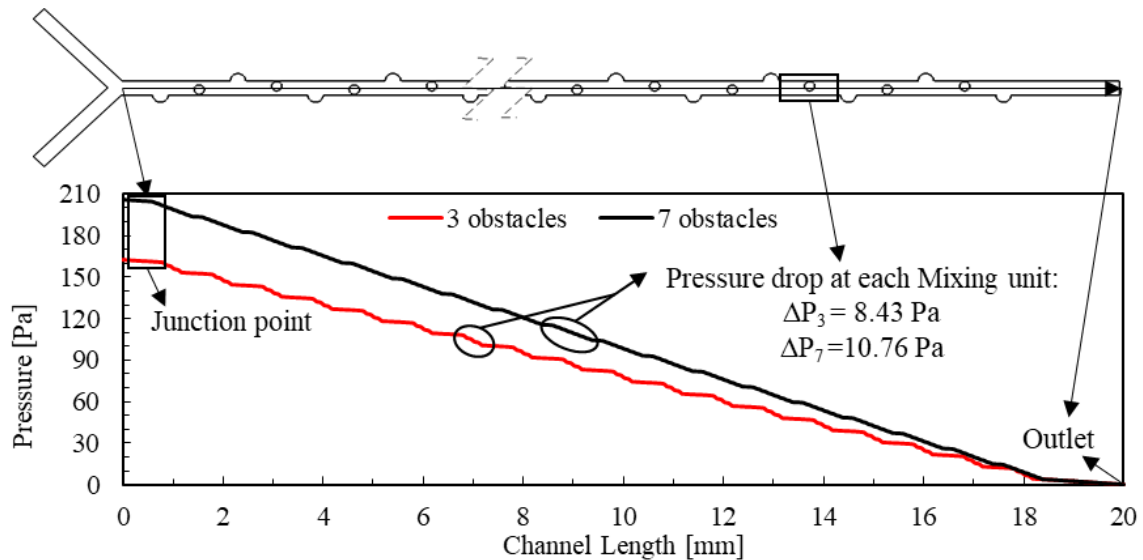


Figure 11 – Pressure difference profile along the channel length.

The graphs show the pressure drop is much steeper overall for the seven-obstacles design. However, the distribution is more uniform than the three-obstacles design. The picture also contains the pressure difference at each mixing unit. At first, this difference is relatively small. However, each time the fluid passes through a mixing unit, it must overcome this pressure drop. Considering that both designs consist of 19 mixing units, the overall  $\Delta P$  difference between them tends to increase linearly as the number of units increases.

The regions where the pressure shows a nearly constant behavior represent the section between grooves and arrangements. Note that for the case of three obstacles, the area of constant pressure is larger due to the greater distance between the cylinder arrangements. Because of this, the pressure difference in the mixing unit is slightly steeper. This phenomenon can indicate both positive and negative aspects. The positive aspect is that this greater distance between the groove and obstacle arrangement contributes to lower  $\Delta P$ , as little energy is required for the fluid to flow, as these regions are predominant in this design. However, the steeper behavior in the area in the obstacle arrangement indicates a higher local pressure drop. The graph in Figure 12 presents information regarding the mixing unit.

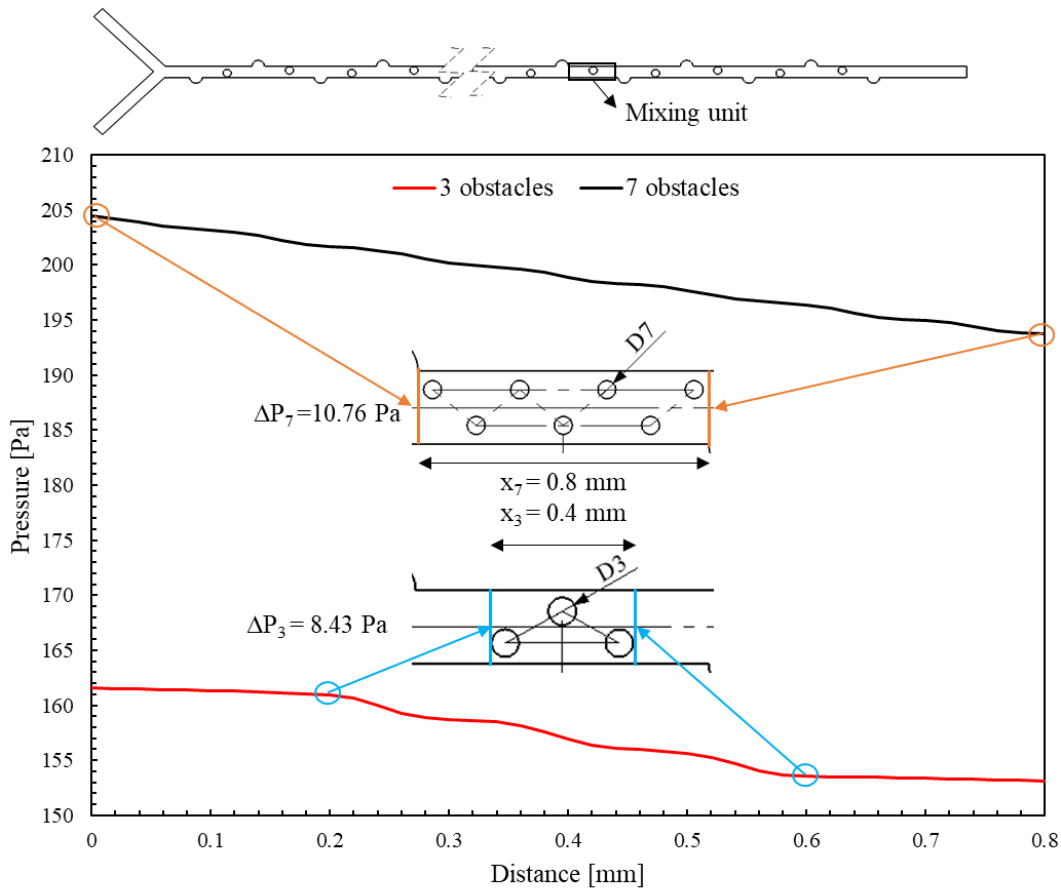


Figure 12 – Local pressure difference at each mixing unit.

As shown in the figure, the actual length of each mixing unit is different because the occupied spacing is larger with more obstacles. In this sense, the localized pressure drops are better distributed. Therefore, the length of each mixing unit is shown in the figure, indicated in the  $x$ -axis.

Analyzing the pressure difference as a function of length, it is possible to determine how much pressure the flow must overcome when passing through each mixing unit through the ratio  $\Delta P_n/x_n$ . Thus, for the case of 7 obstacles, the approximate metric obtained is 13.45 Pa/mm versus 21.08 Pa/mm for the case of 3 obstacles. This analysis reveals that the 3 obstacles mixing unit may be more susceptible to obstructions from particulates from reactions between mixtures or of any other nature, impairing the functionality of the equipment. In this sense, it can be said that the mixing unit of the 7 obstacles design is more efficient than the others. Figure 13 illustrates the velocity magnitude contours and streamlines in the mixing units of the optimal configurations with 3 and 7 obstacles.

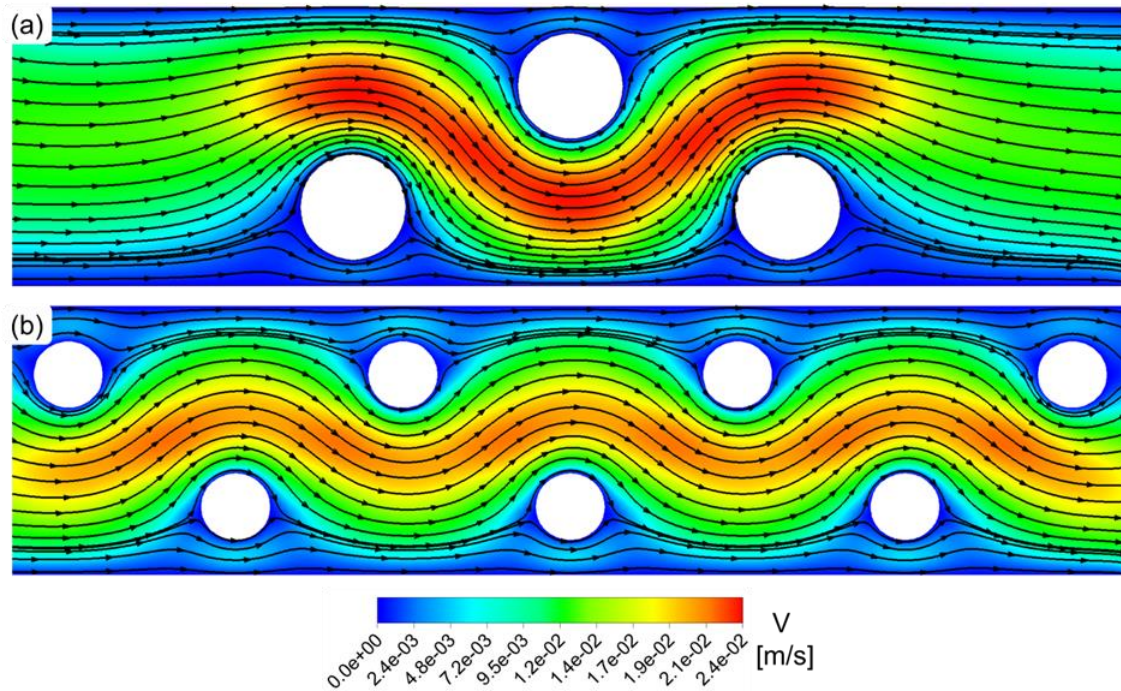


Figure 13 – Streamlines and velocity magnitude contours for optimal configuration at the mixing unit: (a) 3 obstacles; (b) 7 obstacles.

The results show that no recirculation occurred downstream of the obstacles due to the low inertia in the flow ( $Re = 1$ ). Considering the velocity field, the flow is slightly faster in the mixing region (colored red) in design (a). Combining this with the motion of the streamlines, the area between the obstacles is where the velocity changes direction precisely because of the presence of the obstacles, causing one substance to move toward another, essential for the enhancement of mixing.

The correspondence between the velocity (Figure 13) and concentration (Figure 9) contours is remarkable. Mixing is complete (100%) in regions with the highest velocity. With fewer disturbances in the flow, the design with 3 obstacles has lower resistance, resulting in higher velocity in the mixing region, leaving it more intense. In contrast, **in** the 7-obstacles design the fluids change direction more often and perform slightly better in mixing percentage.

Another issue observed in both designs is the low-velocity regions, dark blue, especially in the channel's upper and lower parts. According to the Constructional Theory, regions that do not add to the purpose of the system move it away from **“optimal packing”**. Furthermore, these upper and lower regions contribute little to mixing the substances because the velocity is extremely low, and the interface between one and the other is far away. Therefore, these stagnant zones mix with the central region purely by diffusion,

resulting in a much slower mixing process, giving rise to a high concentration gradient and, consequently, a lower mixing ratio.

A general summary of the cases studied in this work is shown in Figure 14. Figure 14(a) presents the performance of the evaluated designs, and it can be seen that the increase in mixing percentage follows the increase in pressure difference. While the mixing percentage tends to increase uniformly with increasing obstacles,  $\Delta P$  shows a less organized behavior with steep sections, such as the transition of cases from 4 to 5 and 6 to 7 obstacles. Therefore, the best designs are those where the vertical distances between the points of  $\varphi$  and  $\Delta P$  are larger since it is possible to identify the slope of the curve: the steeper the curve of  $\varphi$  relative to  $\Delta P$ , the more efficient the design. Visually, the cases with the greatest vertical distance between the points are the 4 and 6 obstacles.

The geometric evolution plot (Figure 14(b)) shows that  $H$  and  $V$  have an opposite effect as the number of obstacles increases. Thus, several obstacles require reducing horizontal spacing ( $H$ ) for the cluster to fit within the desired spacing. Increasing  $V$  indicates that the obstacles get further apart vertically, compensating for the reduced  $H$ -spacing, which ensures room for the mixture to flow. However, the 6-obstacles design is a non-standard case, as the vertical spacing has decreased while the horizontal spacing has increased from the previous case. This change in the spacing values brought positive aspects to the design since the increase in the mixing percentage offset the rise in the overall pressure difference. Since the 5-cylinder design was identified as the least efficient, this may be a point outside the curve rather than the 6-cylinder design.

Figure 14(c) shows the behavior of the  $MEC$  (in blue) compared to the other references (green and red). In this case, we identify the best designs in which the  $MEC$  remains practically constant in the previous case. As in Figure 14(a), the cases with 4 and 6 obstacles maintain an almost constant  $MEC$  relative to the previous design, providing more options. All proposed designs lay below Ref.2 (red line), which originated the reference geometry.

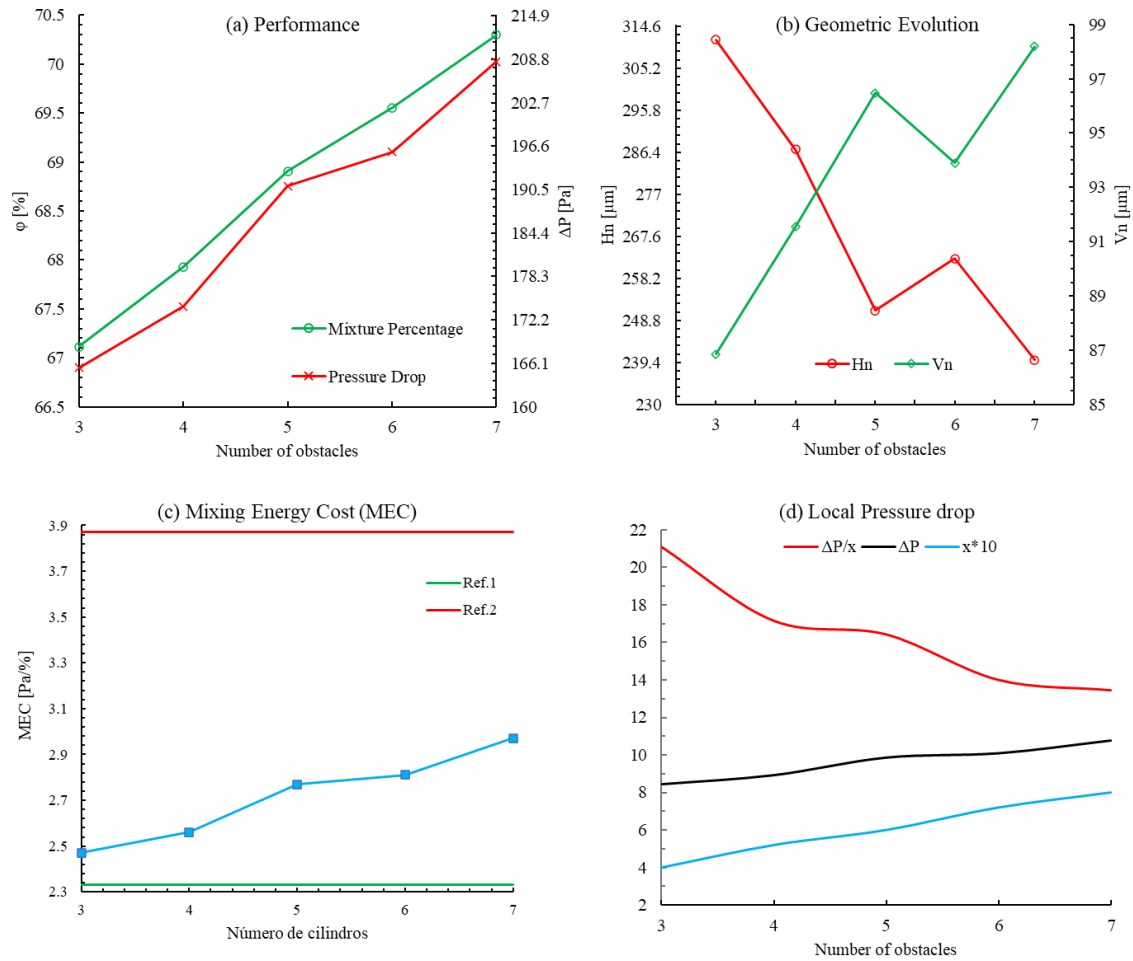


Figure 14 – Overview of the designs studied in this paper: (a) Performance; (b) Geometric evolution; (c) Mixing Energy Cost; (d) Local pressure difference.

Finally, Figure 14(d) presents the difference in local pressure between the designs studied. Again, design 5 gives an undesirable behavior of  $\Delta P/x$ , which is practically constant about the previous case, when the expected would be a more significant reduction. A similar trend is presented between designs 6 and 7. As seen in the earlier analyses, local pressure loss is a negative aspect of the design of a micromixer and should be minimized. The most intense variation is between the designs with 3 and 4 obstacles. This variation can be interpreted as follows: there is not an optimal packing of the mixing unit in Design 3 since the pressure shows more significant gradients in this region. According to Constructal Theory, the optimal geometry is the one that best distributes the imperfections.

Considering the objectives of the work, all the proposed designs met the objective, and, according to the most critical variable ( $\varphi$  or  $MEC$ ), one of the designs can be selected.



However, it is essential to note that there will always be a design that will perform better than another in some specific aspect. In this sense, it is of fundamental importance to analyze the parameters of each design to choose the one that best suits its function.

#### 4 CONCLUSIONS

In this study, an evolutionary design of passive micromixers was performed based on the principles of Constructal Theory. The Constructal Design Method, associated with Response Surface Optimization Method and Computational Fluid Dynamics, was a guide from an initial configuration, morphing to a better performance configuration and adding different degrees of freedom, evolving to even better designs.

The mixing percentage at the channel outlet, the pressure difference from inlet to outlet, and the Mixing Energy Cost (*MEC*) measured system performance. From an evolution level of 3 obstacles per cell, vertical and horizontal distances between obstacles were optimized. Then, more obstacles were added, up to 7 per cell, and obstacles distances were optimized, increasing the mixing percentage for each evolution level.

The initial design results (i.e., three obstacles) showed that vertical distance has a more significant effect on the mixing percentage, as the horizontal distance effect is more substantial on the pressure difference. From the response surfaces, it was possible to notice that the best mixing performance was in an intermediate range of the pressure drop. In terms of *MEC*, this design performed better than previous studies, with a 2.47 and 67.12% mixing index value, satisfying this study's objectives. As for the other designs, the vertical distance effect trend was the same, and the horizontal distance effect on pressure drop was weaker. The latest design evolution (i.e., seven obstacles) achieved the best mixing percentage, 70.30%, meaning an increase of 4.74%, with a pressure drop of 208.49 Pa, 20.24% higher than the initial design. This design returned a *MEC* of 2.97, which is greater than the initial design but lower than the reference design. From this point of view, the three-obstacle design was better. However, considering the local pressure drop gradient, it was observed that the seven-obstacle design had the lowest, 13.45 Pa/mm, which makes it less susceptible to obstructions. At the same time, the highest one, 21.08 Pa/mm, occurred for the three-obstacle design. This analysis revealed a new performance indicator for micromixer designs, which might be valuable in choosing the best design.

Based on the principles of a system's survival by its evolution towards facilitating the flows that keep it alive, this work presented the evolutionary design of a micromixer

from the perspective of the Constructal Theory. When the system had more freedom, it favored its performance. From the Constructal Theory, the best designs presented herein are not final. They could be even better improved if more freedom is given. Adding degrees of freedom can lead to endless possibilities for design evolution. The most straightforward approach would be changing the shape of the obstacles, the shape of grooves, or the dimensions (length, width) while respecting the constraints or relaxing constraints for a greater design range. From the Constructal Law perspective, greater performance designs might be found while the system is free to evolve.

Optimization of the design of micromixers may contribute to increasing the performance of such devices and motivating research on the manufacturing processes of microdevices. With the rapid development of manufacturing processes, building prototypes of optimized micromixers tends to be more feasible and cheaper over the following years. With the possibility of building low-cost prototypes, the optimized designs shall be tested and validated.

Overall, micromixer design brings opportunities regarding applications in various industries such as chemical, pharmaceutical, biotechnology, energy, and food production, being also a test bench for the development of optimization methods, especially for passive micromixers, which rely on geometry to increase the mixture. Also, Constructal Theory brings the idea of evolutionary design for engineering systems. Thus, the proposed and every micromixer design could evolve to achieve better mixing.

## **Acknowledgements**

This work received financial support from the Brazilian agencies CAPES, CNPq and FAPERGS. E.H.T. Cunegatto received a master's degree scholarship from CAPES (Code 001). F. Zinani is a grant holder of CNPq (Proc. No. 311444/2021-0). F. Zinani acknowledges the grant of DIN Senior Visiting Fellow in the Department of Industrial Engineering (DIN), Alma Mater Studiorum, University of Bologna. We gratefully acknowledge the financial support received from the agency FAPERGS (Proc. No. 21/2551-0002169-1). L. Rocha is a grant holder of CNPq (307791/2019-0).

## **REFERENCES**

ANTOIGNOLI, M.; DONATO, L.; GALLETTI, C.; STOECKLEIN, D.; DI CARLO, D.; BRUNAZZI, E. Pre-arranged sequences of micropillars for passive mixing control of water and ethanol, **Chemical Engineering Journal**, v. 461, 2023.

ANTOIGNOLI, M.; STOECKLEIN, D.; GALLETTI, C.; BRUNAZZI, E.; DI CARLO, D. Optimized design of obstacle sequences for microfluidic mixing in an inertial regime, **Lab on a Chip**, v. 20, 2021.

BEJAN, A. Constructal-theory network of conducting paths for cooling a heat generating volume. **International Journal of Heat Mass Transfer**, v. 40, 799-816, 1997.

BEJAN, A.; LORENTE, S. **Design with Constructal Theory**, John Wiley & Sons, Inc, New Jersey, 2008.

BEJAN, A.; ZANE, J.P. **Design in Nature**, Doubleday, New York, 2012.

BEJAN, A. **The Physics of Life: The Evolution of Everything**, St. Martin's Press, New York, 2016.

BORAHHEL, R.S.; ZINANI, F.S.F.; ROCHA, L.A.O.; DOS SANTOS, E.D.; ISOLDI, L.A.; BISERNI, C. Geometric optimization of a rectangular isothermal block inside a lid-driven cavity by means of constructal design. **International Communications in Heat and Mass Transfer**, v. 139, 2022.

CAI, G.; XUE, L.; ZHANG, H.; LIN, J. A Review on Micromixers, **Micromachines** 8, no. 9: 274, 2017.

CELIK, I.B.; GHIA, U.; ROACHE, P.J.; FREITAS, C.J.; COLEMAN, H.; RAAD, P.E. Procedure for Estimation and Reporting of Uncertainty Due to Discretization in CFD Applications, v. 130, **ASME Journal of Fluids Engineering**, 2008.

CETKIN, E.; MIGUEL, A.F. Constructal branched micromixers with enhanced mixing efficiency: Slender design, sphere mixing chamber and obstacles. **International Journal of Heat and Mass Transfer**, v. 131, 2019.

CHEN, X; LV, H. New insights into the micromixer with Cantor fractal obstacles through genetic algorithm. **Sci Rep** 12, 4162 (2022).

CHEN, Y; CHEN, X; LIU, S. Numerical and experimental investigations of novel passive micromixers with fractal-like tree structures. **Chemical Physics Letters**, v. 747, 2020.

CUNEGATTO, E.H.T.; GOTARDO, M.; ZINANI, F.S.F.; Numerical Analysis of Tube Arrangements with One, Two, and Four Degrees of Freedom for Heat Transfer with Pseudoplastic Fluids. **International Journal of Heat and Mass Transfer**, v. 208, 2023.

EL HAMI, A.; POUGNET, P. **Embedded Mechatronic Systems 2**. Elsevier, 2015.

GARCÍA, B.F.; MOUSAVIRAAD, M.; SARAJI, S. Verification and validation for microfluidic CFD simulations of Newtonian and non-Newtonian flows. **Applied Mathematical Modelling**, v. 107, 2022.

HASHEMINEJAD, S.M.; FALLAHI, R. Effects of cylinder cross-sectional geometry and blockage ratio on VIV-based mixing performance in two dimensional laminar channel flow, **Chemical Engineering and Processing – Process Intensification**, v. 177, 2022.

KHAYDAROV, V.; BOROVIKSKAYA, E.S.; RESCHETILOWSKI, W. Numerical and Experimental Investigations of a Micromixer with Chicane Mixing Geometry. **Applied Sciences**, v.8, 2018.

KOUADRI, A.; DOUROUM, E.; LASBET, Y.; NASS, T.T.; KHELLADI, S.; MAKHLOUF, M. Comparative study of mixing behaviors using non-Newtonian fluid flows in passive micromixers. **International Journal of Mechanical Sciences**, v. 201, 2021.

LEE, C.Y; FU, L.M. Recent advances and applications of micromixers. **Sensors and Actuators B: Chemical**, v. 259, 2018.

LEUNG, C.M.; DE HAAN, P.; RONALDSON-BOUCHARD, K. et al. A guide to the organ-on-a-chip. **Nat Rev Methods Primers**, v.2, 2022.

LI, Z.; ZHANG, B; DANG, D.; YANG, X.; YANG, W.; LIANG, W. A review of microfluidic-based mixing methods. **Sensors and Actuators A: Physical**, v. 344, 2022.

LONCHAMPS, P.L.; HE, Y.; WANG, K.; LU, X. Detection of pathogens in foods using microfluidic “lab-on-chip”: A mini review. **Journal of Agriculture and Food Research**. v. 10, 2022.

MAINOCHI, D.O.; AINSTEN, L.; DOS SANTOS, F.P; JUNIOR, M.B.S. Computational fluid dynamics and machine learning as tools for optimization of micromixers geometry. **International Journal of Heat and Mass Transfer**, v. 194, 2022.

MALISKA, C.R. **Transferência de Calor e Mecânica dos Fluidos Computacional**. 2. Ed. Rio de Janeiro: LTC, 2004.

MONTGOMERY, D.C. **Design and Analysis of Experiments**, 8. Ed., John Wiley & Sons, New Jersey, 2012.

NIKPOUR, M; MOHEBBI, A. Optimization of micromixer with different baffle shapes using CFD, DOE, meta-heuristic algorithms and multi-criteria decision making. **Chemical Engineering & Processing: Process Intensification**, v. 170, 2022.

ORTEGA-CASANOVA, J. Application of CFD on the optimization by response surface methodology of a micromixing unit and its use as a chemical microreactor. **Chemical Engineering & Processing: Process Intensification**, v. 117, 2017.

PATANKAR, S. V. **Numerical Heat Transfer and Fluid Flow**. McGraw-Hill, New York, 1980.

RAHMANNEZHAD.J.; MIRBOZORGI, S.A. CFD analysis and RSM-based design optimization of novel grooved micromixers with obstructions, **International Journal of Heat and Mass Transfer**, v. 140, p. 483-497, 2019.

ROCHA, L.A.O.; LORENTE, S.; BEJAN, A. **Constructal theory in heat transfer**, in: KULACKI, F.A. (Ed.), **Handb, Therm. Sci. Eng**, Springer Cham, 2018.

SANTANA, H.S.; HADDAD, V.A.; CALVO, P.V.C.; PALMA, M.S.A.; DA SILVA, A.G.P.; NORILER, D.; TARANTO, O.P.; SILVA, J.L. Design, optimization and scale-up of a new micromixer design based on plate column for organic synthesis, **Chemical Engineering Journal**, v. 446, 2022.

SANTANA, H.S.; SILVA JR, J.L.; TARANTO, O.P. Optimization of micromixer with triangular baffles for chemical process in millidevices, **Sensors and Actuators B: Chemical**, v. 281, 2019.

SAORIN, G.; CALIGIURI, I.; RIZZOLIO, F. Microfluidic organoids-on-a-chip: The future of human models. **Seminars in Cell & Developmental Biology**. 2022.

WANG, L.; LIU, D.; WANG, X.; HAN, X. Mixing enhancement of novel passive microfluidic mixers with cylindrical grooves. **Chemical Engineering Science**, v. 81, 2012.

WASHINGTON, S.P.; KARLAFTIS, M.G.; MANNERING, F.L. **Statistical and Econometric Methods for Transportation Data Analysis**, 2. Ed., Chapman & Hall/CRC, 2011.